Colloidal stability of capped silver nanoparticles in natural organic matter-containing electrolyte solutions

Leonardo Gutierrez, Andreas Schmid, Noor Zaouri, Daniel Garces, Jean-Philippe Croué

Colloidal stability of capped silver nanoparticles in natural organic matter-containing electrolyte solutions

Submitted to

NanoImpact Journal

April 2020

Leonardo Gutierrez[1,6*], Andreas Schmid[2], Noor Zaouri[3], Daniel Garces[4], Jean-Philippe Croue[5,*]

[1] Facultad del Mar y Medio Ambiente, Universidad del Pacifico, Ecuador

[2] Department of Environmental Systems Science, Swiss Federal Institute of Technology ETH, Zurich, Switzerland

[3] Water Desalination and Reuse Center, King Abdullah University of Science and Technology, Saudi Arabia

[4] Facultad de Ciencias de la Tierra, Escuela Superior Politecnica del Litoral

[5] Institut de Chimie des Milieux et des Matériaux, IC2MP UMR 7285 CNRS, Université de Poitiers, France

[6] Particle and Interfacial Technology Group, Department of Applied Analytical and Physical Chemistry, Ghent University, Coupure Links 653, 9000, Ghent, Belgium

* Corresponding author: Tel.: +32 (0) 468358104
E-mail address: leo.gutierrez@upacifico.edu.ec
jean.philippe.croue@univ-poitiers.fr

28 pages, 6 figures, and a Supporting Information (SI) section are included in the current manuscript.

Abstract

Due to their increased production and commercial applications, capped silver nanoparticles (AgNPs) have inevitably found their way into aquatic ecosystems. The mobility (fate/transport), bioavailability, reactivity, and toxicity of capped AgNPs are highly influenced by their colloidal stability. This study investigated the aggregation kinetics and interfacial interactions of tannic acid (TA)-coated or silica-coated AgNPs in natural organic matter (NOM)-containing electrolyte solutions by time-resolved dynamic light scattering and atomic force microscopy. Three well-characterized NOM fractions of different characteristics were selected. In Na^+-solutions, the polymeric TA induced more stability to AgNPs than the hard silica coating. Although all NOM fractions weakly interacted with TA even at high Na^+ concentrations, these organics adsorbed on the silica-coated AgNPs; thus, inducing stability. Humic fractions provided higher colloidal stability due to stronger electrostatic/steric interactions. Ca^{2+} increased the aggregation kinetics of both capped nanoparticles in the absence and presence of NOM. However, the aggregation kinetics of TA-coated AgNPs in humic NOM-containing solution were higher than those of non-humic due to a higher content of deprotonated carboxyl groups and cation bridging mechanisms. The knowledge compiled in this study would assist in understanding and predicting the fate and transport of capped nanoparticles in natural aquatic systems of different compositions.

Keywords: capped silver nanoparticles; natural organic matter; colloidal stability; aggregation; dynamic light scattering.

1. Introduction

The production of engineered silver nanoparticles (AgNPs) in the industry has rapidly increased due to their broad commercial applications (e.g., cosmetics, paints, food industry, medical fields, and electronics) [1-3]. As a result, AgNPs have inevitably found their way into aquatic ecosystems [4, 5]. The toxic impact of AgNPs would cause adverse effects on microbial communities, aquatic organisms, and human health through possible chemical or physical transformation reactions (i.e., sulfidation, dissolution, aggregation); thus, leading to changes in crucial ecosystem processes [6, 7]. Remarkably, the bioavailability, reactivity, mobility, and toxicity of manufactured AgNPs are highly influenced by their colloidal stability.

Colloidal stability in an aqueous solution is defined as the ability of particles to resist aggregation over a specific time and is influenced by solution conditions (e.g., pH, ionic strength-IS, electrolyte composition, and presence of natural organic matter-NOM) and type of capping agents [8-10]. These capping agents (i.e., typically synthesized with different organic surface coatings) are usually negatively charged species or long and hydrophilic polymers that prevent aggregation of AgNPs by providing additional electrostatic, steric, or electrosteric repulsive forces [11, 12]. Polyvinylpyrrolidone (PVP), polyethylene glycol (PEG), silica, tannic acid (TA), and citrate are commonly used capping agents due to their high chemical stability, low toxicity, and high solubility in polar solvents [12-18]. However, these capping agents would interact with other water constituents (e.g., NOM, electrolytes), leading to changes in the physicochemical properties of AgNPs surface (i.e., functionalities, surface charge, hydrophobicity) [19, 20].

NOM and electrolytes are ubiquitous constituents in aquatic ecosystems that influence the fate and transport of AgNPs [9, 21]. Previous studies have investigated the interactions between

NOM, electrolytes, and capped AgNPs using varied techniques, e.g., Time-Resolved Dynamic Light Scattering (TR-DLS), Flow Field-Flow Fractionation, or Quartz Crystal Microbalance. Briefly, bare AgNPs readily aggregate under low NaCl and $CaCl_2$ concentrations (i.e., critical coagulation concentration-CCC: 40 and 2 mM, respectively), indicating their low stability in solution [22]. Although capping agents prevent AgNPs from aggregating through steric hindrance or additional electrostatic repulsion, the presence of high electrolyte concentrations or divalent cations can lead to colloidal instability by charge screening or cation bridging, respectively [13, 23, 24]. For instance, the CCC of PVP-coated and citrate-coated AgNPs in $CaCl_2$ solution were lower than that in NaCl solutions at similar IS [20, 24]. Other studies have also observed enhanced aggregation of capped AgNPs in divalent cation solutions [12, 19]. However, NOM interactions with AgNPs would increase colloidal stability. PVP-coated and citrate-coated AgNPs were stabler in humic acid (HA)-containing NaCl solutions, while Ca^{2+} cations induced enhance aggregation [20, 24]. HA in solution hindered the deposition of these capped AgNPs on silica surfaces, confirming their mobility in NOM solutions under environmentally relevant conditions [13].

Remarkably, due to the: a) increased production of capped AgNPs, and b) their environmental impacts on natural water systems, there are at present concerted efforts to synthesize non-toxic "green" AgNPs. Tannic acid (TA, highly biocompatible compound) is being increasingly used as a stabilizing agent [15, 18]. TA is a weak acid and polyphenolic compound (hydrolyzed tannin) of antimutagenic, anticancer, and antioxidant properties [25, 26]. Similarly, silica (i.e., a ubiquitous mineral on earth) is also widely used as a capping agent for AgNPs in electronics, optics, and biochemistry fields [16, 17]. Unlike their counterparts (e.g., citrate-, PVP-, and PEG-coated AgNPs), the colloidal stability of TA-coated and silica-coated AgNPs in NOM-containing

electrolyte solutions has not been studied. This new knowledge would assist in understanding and predicting their fate and transport in natural aquatic systems.

This study investigated the interfacial interactions and aggregation behavior of TA-coated and silica-coated AgNPs in the presence of NOM and under different solution conditions. TA and silica capping agents were selected due to their increased production and commercial applications, and greener approach. Three well-characterized NOM isolates of different properties were selected: two river humic fractions from Gartempe River (France) and Colorado River (USA), and a hydrophilic isolate from Ribou River (France). Specifically, i) the interactions between NOM and the polymeric surface of TA-coated AgNPs or the hard surface of silica-coated AgNPs (i.e., hard vs. polymeric coatings are compared for the first time), and ii) the influence of solution conditions (type and concentration of cations) were investigated. TR-DLS technique was used to investigate aggregation kinetics of the capped AgNPs in NOM-containing electrolyte solutions. Because NOM changes the surface properties of the capping agents upon adsorption, Atomic Force Microscopy (AFM) in contact mode was used to study the contributions of van der Waals, electrostatics, and steric mechanisms of every NOM isolate during interfacial interactions. These experimental conditions were carefully selected to mimic real environmental scenarios. The knowledge compiled would assist in identifying research directions to understand and predict the fate and transport of capped nanoparticles in natural aquatic systems of different compositions.

2. Materials and Methods

2.1. Nanoparticles samples, reagents, and solution chemistries

Electrolyte solutions for NOM stock preparation, AFM, and TR-DLS experiments were prepared with ultrapure water (resistivity of 18 MΩ·cm, Millipore, USA) and analytical grade agents (i.e.,

115 NaCl, $CaCl_2$, NaOH, $FeCl_3$, $NaNO_3$), and subsequently filtered through a 0.22 μm membrane.
116 The iron oxide solution used for the layer-by-layer coating procedure of AFM colloidal probes
117 was prepared by increasing the pH of a 10 mM $FeCl_3$ solution to 7 by small additions of NaOH,
118 as described elsewhere [27, 28]. Spherical silica-coated AgNPs (TEM silver core diameter:
119 70±10 nm, and silica shell thickness: 20±5 nm) and spherical TA-coated AgNPs (TEM diameter:
120 100±9.4 nm) were obtained from NanoXact (Nano-Composix, USA). Both capped nanoparticles
121 stocks were subjected to a dialysis-filtration process in a 1 mM $NaNO_3$ solution to remove
122 colloidal TA and dissolved silica species, using an Amicon cell (Millipore, USA). After this
123 purification process, the final concentration of both stocks of nanoparticles was approximately
124 20 ppm. Additionally, the quality of the stocks of nanoparticles was monitored for the duration
125 of this investigation by hydrodynamic diameter and electrophoretic mobility measurements.

126 ***2.2. Origin, characteristics, and NOM stock preparation***

127 The NOM isolates selected for this investigation were obtained from three different surface
128 waters: a) Gartempe-HPO: a hydrophobic (HPO) NOM fraction extracted from a black water of
129 high humic content (i.e., high specific ultraviolet absorbance-SUVA) from Gartempe River,
130 France, b) Colorado-HPO: an HPO isolate collected from Colorado River, USA (low humic
131 content water), and c) Ribou-HPI: a biopolymer/hydrophilic (HPI) fraction from Ribou River,
132 France (non-humic, low SUVA water). These three fractions were isolated following the
133 comprehensive protocol described elsewhere [29], and have been rigorously characterized and
134 described in previous investigations and summarized in the SI section [20, 27, 30, 31]. The NOM
135 stock solutions were prepared by dissolving a NOM fraction in 1 mM NaCl solution, stirred
136 overnight, and filtered through a 0.45 μm membrane. The monodispersion of the dissolved NOM

was evidenced by TR-DLS (Figure S1). The final concentration of the NOM stock was approximately 100 mg C/L.

2.3. Electrophoretic Mobility (EPM) of the Natural Organic Matter isolates

The EPM of NOM samples was measured using a ZS ZEN3600 Zetasizer (Malvern, UK) and following the protocol described elsewhere [32]. Briefly, silica particles (1.6 μm in diameter, Polysciences, Warrington, PA) were coated with Gartempe-HPO, Colorado-HPO, or Ribou-HPI by the layer-by-layer method and using positively-charged iron oxide as an intermediate layer [27]. 1 mL clear disposable zeta cells (DTS1060C, Malvern, UK) were used to measure the EPM of NOM-coated silica particles under: 1, 3, 10, 30, and 100 mM NaCl solutions, and 0.33, 1, 3.33, 10, and 33.3 mM $CaCl_2$ solutions at ambient pH. These solution conditions are respectively equivalent in terms of Ionic Strength. A minimum of three measurements was collected for every solution condition. EPM values were converted to zeta potential by the Smoluchowski equation using Dispersion Technology Software (v5.10, Malvern, UK). The data sets obtained were pooled and the average results, including standard deviation, were presented in this study.

2.4. Interaction forces between NOM fractions and mica surface

AFM was used to study the dominant interacting mechanisms (i.e., electrostatic, van der Waals, or steric interactions) between NOM and mica surface as a function of solution conditions. Mica was selected as a model surface due to its high electronegativity (i.e., highly negatively-charged surface). Based on Coulomb's law, the electrostatic repulsive forces between NOM isolates and mica surface (i.e., forces proportional to the product of their charges) would be clearly detected in the force vs. distance profiles generated by the AFM at different ionic strengths (IS) [27]. Steric repulsive forces would also be detected and discriminated against long-ranged exponential electrostatic forces [33]. These results would assist in: i) identifying and measuring the electrostatic and steric repulsive forces generated by each NOM fraction as a function of their

161 physicochemical characteristics and solution condition, and thus, ii) understand the interactions
162 between NOM and capped AgNPs.
163 A Dimension FastScan AFM (Bruker, USA) with an Icon Head was used to measure interaction
164 forces during the approaching regime. A ~20 μm silica sphere glued on a silicon nitride
165 cantilever with a manufacturer-reported spring constant of 0.24 N/m (SNL, Bruker, USA) was
166 used as an AFM colloidal probe and will be termed as AFM probe for the rest of this
167 investigation. These sensitive AFM probes of low spring constant/stiffness were selected to
168 record small forces originated from considerably small deflections of the cantilever during
169 interactions with soft materials (e.g., organic matter structures). The calibration of the AFM
170 probes was conducted as follows. Briefly, the deflection sensitivity of the AFM probes was
171 measured in air conditions and using freshly-cleaved mica as a control substrate. The spring
172 constant (k) of the cantilevers was determined by the Thermal Tuning method, where deflection
173 (V) was converted to force (nN) in accordance with Hooke's law [34]. No significant deviation
174 from the specification of the manufacturer was observed. The NOM coating of the AFM probes
175 was conducted following the layer-by-layer protocol and using positively-charged iron oxide as
176 an intermediate layer, as previously described [27]. As a control experiment, the spring constant
177 of the NOM-coated AFM probes was measured and compared to those of the silica colloidal
178 probes, where no significant difference was observed. These results indicate no impact of the
179 NOM coating on the nanomechanical properties of the cantilevers. A minimum of 10 force
180 profiles were recorded for every NOM sample at 1, 10, and 100 mM NaCl-containing solutions.
181 The forces recorded were normalized by the radius of the colloidal probe (F/R), presented in
182 units of mN/m, and modeled by Classic and Extended Derjaguin-Landau-Verwey-Overbeek
183 (DLVO) theory (section 2.5). Force profiles were not performed in $CaCl_2$-containing solutions

because the DLVO theory does not account for specific interactions and complexation between Ca^{2+} cations and functional groups.

2.5. Modeling of interacting forces between organics and surfaces: Classic and Extended Derjaguin-Landau-Verwey-Overbeek (DLVO) theory.

During approaching regime, interaction force vs. distance curve profiles were modelled following: a) Decay length, b) Classic DLVO, and c) Extended DLVO theory. Briefly, experimental Decay length follows an exponential decay described by the equation: $F = F_o exp(-\kappa d)$, where F is the interaction force, F_o is a pre-exponential constant physically described as the force at contact, κ^{-1} is the interaction force decay length, and d is the separation distance [34]. Approaching curves were individually analyzed to extract F_o and κ^{-1} at every solution condition. Additionally, Classic DLVO theory is described as the sum of van der Waals (vdW) and electrostatic double-layer interactions (i.e., considering a sphere and an infinite planar surface) as: $F_{DLVO} = F_{vdW} + F_e$; where A_{123} is the Hamaker constant, r is the radius of the colloidal AFM probe, d is the separation distance between the AFM colloidal probe and mica surface, ψ_t and ψ_s are the surface potentials of the NOM-coated AFM colloidal probe and model mica surface, respectively, κ is the inverse Debye length, k is the Boltzmann constant, e is the electron charge, T is the absolute temperature, z is the valence, ε is the dielectric constant of the solution, and ε_o is the dielectric permittivity of vacuum (Eq. 1-2) [35].

$$F_{vdW} = \frac{A_{132}}{6}\left[-\frac{r}{d^2} - \frac{r}{(d+2r)^2} + \frac{2r}{d(d+2r)}\right] \quad (1)$$

$$F_e = 4\pi\varepsilon\varepsilon_o(\kappa r)\left(\frac{kT}{ze}\right)^2 \psi_t\psi_s\left[\frac{exp(-\kappa rd)}{1+exp(-\kappa rd)} - \frac{(\psi_t-\psi_s)^2}{2\psi_t\psi_s} * \frac{exp(-2\kappa rd)}{1-exp(-2\kappa rd)}\right] \quad (2)$$

$$F_{XDLVO=}F_{DLVO} + F_o \exp\left(-\frac{h}{\lambda}\right)$$

Besides vdW and electrostatic forces, an extended DLVO model considered the contribution of steric repulsive forces as previously described (Eq. 3) [36]. λ is a characteristic Decay length of possible steric nature. All the experimental Force-Distance profiles were modeled using nonlinear regression by OriginPro v.2018, providing a physical description of the influence of electrostatics, vdW, and steric repulsive forces during NOM interactions with surfaces.

2.6. Aggregation Kinetics of capped AgNPs in NOM-Containing Electrolyte Solutions

The stability of TA-coated and silica-coated AgNPs was studied by the TR-DLS technique in NOM-containing electrolyte solutions using a ZS ZEN3600 Zetasizer (Malvern, UK) and low volume plastic disposable cuvettes (ZEN112, Malvern, UK). The intensity-weighted hydrodynamic diameter (D_h) of capped AgNPs was calculated by second-order cumulant analysis using Dispersion Technology Software (v5.10, 2008, Malvern, UK) as previously described [37]. The initial hydrodynamic diameter (D_{ho}) of capped AgNPs was measured by diluting the stock suspensions in a 1 mM NaCl solution to a final concentration of 1 ppm and to a final volume of 500 µL and was used as a baseline for the following aggregation kinetics experiments. During TR-DLS experiments, TA-coated or silica-coated AgNPs were added to the electrolyte solution to a final concentration of 1 ppm and to a final salt concentration of 1, 3, 10, 30, 50, and 100 mM NaCl, or 0.33, 1, 3.33, 10, 16.6, and 33 mM $CaCl_2$ (i.e., selected as representative for fresh and brackish water sources), gently shook, and placed in the Zetasizer equipment for immediate measurement. The autocorrelation functions were accumulated for 20 s, and the measurements extended over 1 h. Similar to the previous experimental condition, capped AgNPs and NOM were simultaneously added to electrolyte solution to a final concentration of 1 ppm and 10 mg C/L, respectively. The latter condition was selected based on the NOM concentration found in their respective aquifers [38, 39]. The experimental aggregation kinetic rate constant (k_{11}) of capped AgNPs in an electrolyte solution or NOM-containing

electrolyte solution was calculated during early stages of aggregation as the initial rate of increase in the nanoparticles hydrodynamic diameter (D_h) as a function of time (t) (i.e., slope), up to the point at which D_h reaches the relative hydrodynamic diameter of $1.38D_{ho}$, as described elsewhere [37]. The experimental aggregation kinetic rate constant (k_{11}) of capped AgNPs provided fundamental information of diffusion-limited and reaction-limited regimes (i.e., favorable/unfavorable aggregation) as a function of solution conditions.

3. Results and Discussion

3.1. Electrophoretic mobility of NOM fractions

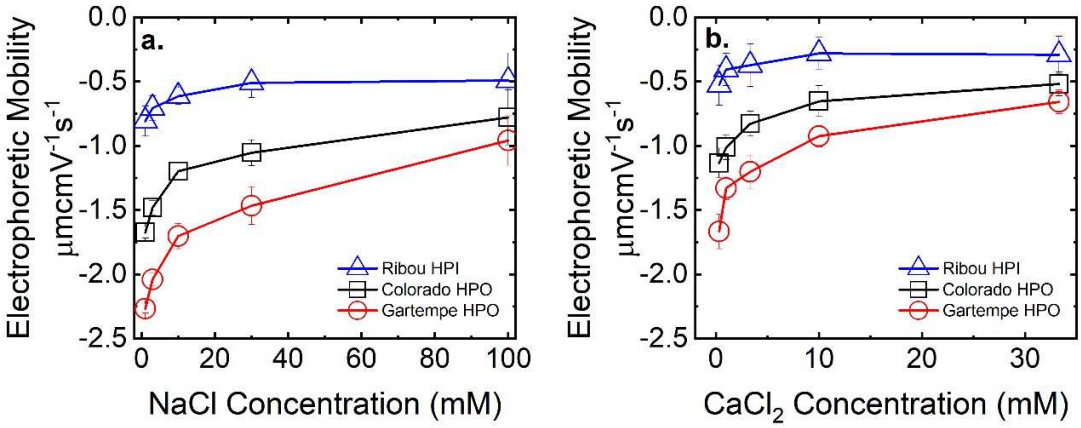

Figure 1: EPM of Ribou-HPI, Colorado-HPO, and Gartempe-HPO in a) 1, 3, 10, 30, and 100 mM NaCl and b) 0.33, 1, 3.33, 10, and 33.3 mM $CaCl_2$ solutions

The EPM of the three organic fractions were negative throughout the entire NaCl and $CaCl_2$ concentration range tested (Figure 1). In NaCl solutions, the EPM of the three isolates became less negatively-charged with increasing ionic strength (Figure 1a). Nevertheless, the magnitude of the negative charge of these isolates followed the order of Gartempe HPO > Colorado HPO > Ribou HPI. These differences in EPM would be fundamental during interactions with the capped AgNPs and ions in solution and can be explained by the physicochemical characteristics of the NOM fractions, summarized as follows (Table S1-S2) [20, 27, 30, 31]. Briefly, Gartempe-HPO

(i.e., hydrophobic acids) was found rich in carboxylic acids (i.e., deprotonated at neutral pH conditions due to their low pKa [40], and main contributor to the charge of the NOM) and aromatic ring structures, while signals of carbohydrates and proteins were almost absent in ^{13}C-NMR and FT-IR spectra. Also, this isolate presented a predominance of fulvic acid structures, typical of surface water humic substances. Conversely, Ribou HPI (i.e., hydrophilic colloids) showed a weak presence of aromatic ring structures and carboxyl groups (i.e., explaining its low EPM). Interestingly, a high organic nitrogen content, a large presence of proteins, polysaccharides, and aminosugars were observed. Carbohydrates (i.e., aliphatic structures and alcoholic functional groups) constituted a major fraction in this isolate (analysis is provided in the SI section). Alcoholic groups would not contribute to the charge of the molecule due to its high pKa [40]; however, they play a role during acid-base interactions. Additionally, through contact angle measurements and the calculation of interfacial free energy of interaction with water (ΔG_{121}), previous studies have reported the higher hydrophilicity of -OH than of -COOH groups [41, 42]. These characteristics conferred Ribou-HPI of a strong hydrophilic character. Colorado-HPO also showed a predominance of fulvic acid structures, however, derived from terpenoids. Although significant, the phenolic, aromatic, and carboxyl group contents were lower than that of Gartempe-HPO. Remarkably, this fraction showed abundant polysaccharides moieties and high alcoholic group content [30, 31]. Similarly, the negative charge of the three organic fractions decreased with increasing $CaCl_2$ concentration in solution (Figure 1b) and also followed the order of Gartempe HPO > Colorado HPO > Ribou HPI. However, the magnitude of the negative charge of the organics in $CaCl_2$ solutions was lower than those in NaCl solutions throughout the whole range of ionic strength. Previous studies have observed similar trends [20, 32, 43]. Ca^{2+} would exert an influence on the surface properties of the organics, possibly through

cation complexation with deprotonated carboxyl groups [44]. This latter observation would indicate the importance of the characteristics of these organic fractions during interactions with other surfaces and colloids in solution (e.g., capped AgNPs). The abovementioned characteristics (e.g., aromaticity, aliphaticity, carbohydrate/protein content, carboxyl, alcoholic, methyl functional groups) defined the hydrophobic and hydrophilic nature of the NOM fractions; and thus, would exert an impact during interactions with ions and the capping agents of AgNPs.

3.2. Interfacial interactions between NOM and mica surface

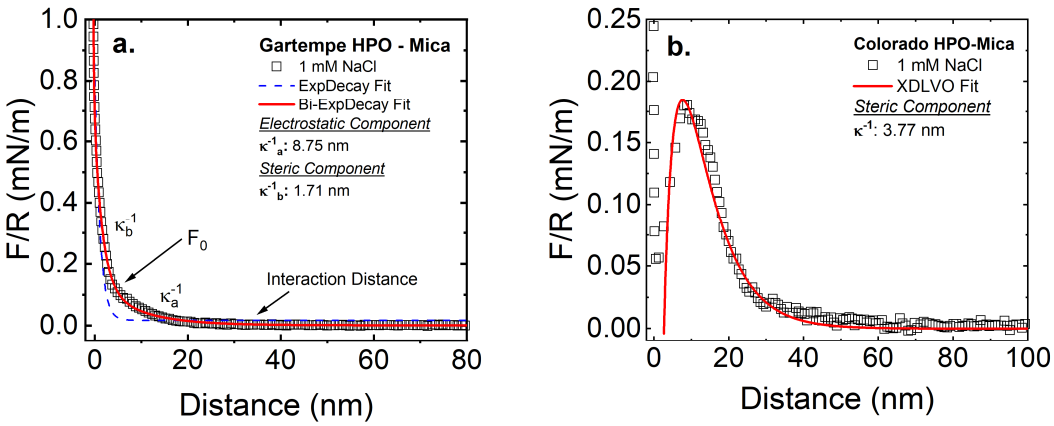

Figure 2: Representative force vs. distance curves during approaching regime between the mica surface and a) Gartempe HPO or b) Colorado HPO-coated colloidal probe. The forces were normalized by the radius of the colloidal probe (F/R) and presented in units of mN/m.

NOM changes the surface properties of the capping agents upon adsorption and, thus, influences the interfacial interactions of the capped nanoparticles with other components of aquatic systems (e.g., colloids, ions). Therefore, AFM in contact mode was used to study the contributions of van der Waals, electrostatics, and steric mechanisms of every NOM isolate during interfacial interactions. The force vs. distance curves during approaching regime between the mica surface and the three organic isolates showed different profiles. Briefly, during Gartempe HPO approaching to the mica surface, long-ranged repulsive forces were initially recorded at an

interaction distance of approximately 30 nm in 1 mM NaCl-containing solution (Figure 2a). These repulsive forces increased with decreasing interaction distance, following an exponential profile until a linear response of the cantilever (i.e., constant compliance region) and overcoming attractive vdW forces. The magnitude of these repulsive forces decreased with increasing NaCl concentration in solution due to the: a) charge screening and b) compression of polymeric structures of the organic fraction, thus, resulting in decreased inter/intramolecular repulsive forces as previously suggested [45]. Regardless of the ionic strength of the solution, no jump-into-contact effect was observed between Gartempe HPO and the mica surface in all the force curves recorded. A jump-into-contact occurs when the spring constant of the cantilever is exceeded by the gradient of the attractive forces between the surface and colloidal probe during approaching regime [46]. An exponential decay fit could not successfully describe the profile of the approaching curves (Figure 2a); thus, indicating additional interactive mechanisms between Gartempe HPO and mica besides electrostatics. Nevertheless, the force profile was described by a bi-exponential decay fit (Figure 2a), indicating two regions of different interacting mechanisms. Additional details regarding decay and Debye length calculations are provided in the SI section. Previous studies have observed similar trends in the force vs. distance approaching curves between NOM-coated surfaces [33, 47]. Two decay lengths were extracted, where the first decay length would correspond to long-ranged interactions of electrostatic nature, while the second decay length would be assigned to repulsive steric forces caused by the compression of the polymeric structures of Gartempe HPO. Specifically, the magnitude of the decay length of the first region was highly dependent on the solution chemistry and was close to the theoretical Debye length (e.g., 8.87, 4.39, and 2.02 nm vs. 9.84, 3.11, and 0.98 nm for 1, 10, and 100 mM NaCl, respectively) [35]. This latter observation is consistent with the

physicochemical characteristics of this organic fraction and its high EPM (Figure 1). Conversely, the decay length of the second region showed lower values and less sensitive to solution conditions (e.g., 1.68, 1.51, and 0.89 nm for 1, 10, and 100 mM NaCl, respectively).

Similarly, the force vs. distance curves between Colorado HPO and the mica surface also showed increasing repulsive forces with decreasing interaction distance following a pseudo-exponential decay, possibly of electrostatic and steric nature (Figure 2b). Nevertheless, jump-into-contact events were recorded following the long-ranged repulsive forces, suggesting another type of dominant interacting mechanism at short distances. Jump-into-contact events were observed in every force-curve irrespective of ionic strength in solution. The gradient of the attractive forces inducing jump-into-contact would be caused by a combination of low electrostatic repulsive forces, attractive vdW forces, and acid-base interactions (i.e., hydrogen bonds between hydroxyl groups present in Colorado HPO and electronegative elements in the mica surface), as previously suggested [45, 48]. Specifically, Colorado-HPO showed polysaccharides moieties and alcoholic group content (i.e., absent in Gartempe-HPO); thus, contributing to its affinity towards mica. The magnitude of the decay length corresponding to the long-range electrostatic repulsive forces was also dependent on the solution chemistry and close to the theoretical Debye length (e.g., 8.21 and 2.78 for 1 and 10 mM NaCl, respectively). Moreover, the XDLVO model assisted in elucidating the contribution of the short-range forces of possible steric nature (Eq. 3). The characteristic Decay length (λ) extracted at 1 mM NaCl (i.e., 3.77 nm) was higher than that of Gartempe HPO (Figure 2b), suggesting steric repulsive forces as an additional mechanism interacting between Colorado NOM and the mica surface. Additional details regarding XDLVO calculations are provided in the SI section. On the other hand, jump-into-contact events have been recognized as unstable regimes that prevent the accurate measurement of attractive forces and induce

misinterpretations regarding zero-distances [34]; thus, difficulting the modeling and physical description of attractive short-range forces. Thus, the current study did not further study this phenomenon.

Conversely, the force vs. distance curves between Ribou HPI and mica surface showed no repulsive forces even at low ionic strength (1 mM NaCl), where the screening of charges is not significant (Figure S2). This low electrostatic repulsion (i.e., low electrostatic repulsive forces below the detection limit of the AFM) would be explained by the physicochemical characteristics of this fraction and also clearly evidenced by its low EPM (Figure 1). Specifically, this fraction is characterized by the weakest presence of carboxyl groups among the three NOM selected. Nonetheless, polysaccharides, aminosugars, aliphatic structures, and alcoholic functional groups constituted a major fraction contributing to the hydrophilic character of Ribou HPI (analysis is provided in the SI section), and thus, to the high affinity to the super hydrophilic mica surface. As a consequence, jump-into-contact events were recorded at all solution conditions, possibly caused by a combination of attractive vdW forces and strong acid-base interactions between the dominant alcoholic groups in the structure of Ribou HPI and electronegative elements in the mica surface [48].

In summary, the combination of high electrostatic charge, steric forces induced by its polymeric nature, and its high aromatic/phenolic carbon content would cause the high repulsion and lack of jump-into contact events between Gartempe-HPO and the highly electronegative and hydrophilic mica. On the other hand, the lower charge, aromatic carbon, and phenolic content, in addition to abundant polysaccharide moieties and alcoholic groups, would induce short-range attractive forces of acid-base nature that caused jump-into-contact events between Colorado-HPO and

mica. Conversely, the hydrophilic nature and considerably low charge of Ribou HPI would induce jump-into contact events and the lowest repulsion forces to mica (i.e., high affinity).

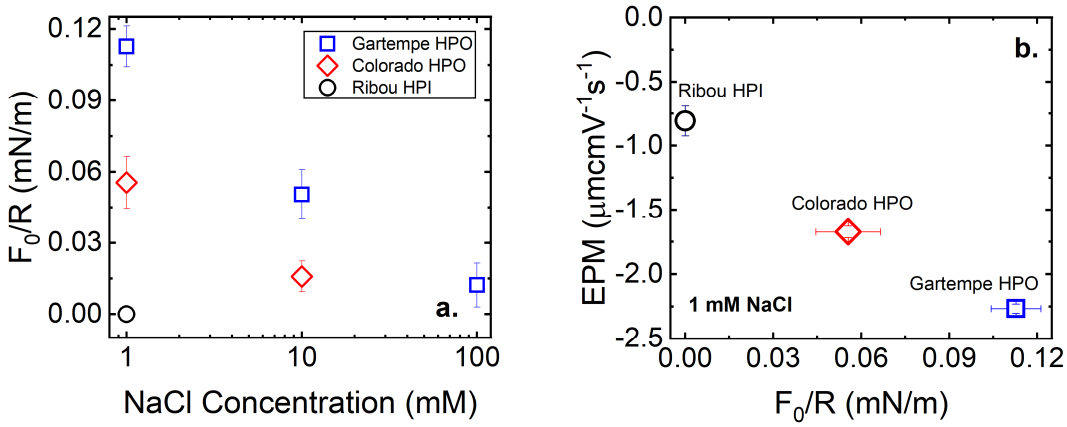

Figure 3: a) Repulsive electrostatic forces between NOM isolates and mica surface in NaCl solutions of different ionic strengths. b) Zeta potential of NOM isolates vs. repulsive electrostatic forces between NOM isolates and mica surface in a 1 mM NaCl solution. The forces were normalized by the radius of the colloidal probe (F/R) and presented in units of mN/m.

The force at contact (F_o) was extracted from the fitting of the electrostatic component (i.e., long-range interactions) of the approaching curve of Gartempe HPO, Colorado HPO, and Ribou HPI, as previously described [33, 47], and plotted against the NaCl concentration (Figure 3a). This force at contact (F_o) would represent the approximate maximum electrostatic repulsive force recorded between the NOM-coated AFM probe and the mica surface before contact. Due to well-known uncertainties (e.g., heterogeneity in the thickness of the NOM-coating layer, the molecular weight of the NOM structures, molecular arrangements within the coating layer), determining the exact point of contact has been previously reported as challenging [49]. Due to its extremely low magnitude, the F_o value of Ribou HPI at 1 mM NaCl was set as zero nN (i.e., no repulsive force was detected prior jump-into-contact events). The magnitudes of F_o for the three organic fractions followed the order of: Gartempe HPO>Colorado HPO>Ribou HPI (i.e., consistent with their respective physicochemical characteristics) and sharply decreased with

increasing ionic strength in solution, indicating charge screening (Figure 3a). Additionally, a strong correlation between the EPM and F_o values of the three organics was observed (Figure 3b); thus, indicating the importance of the physicochemical characteristics of these organics during long-range electrostatic interactions. Electrostatic forces play a key role in the energy barriers between surfaces during interactions in solution [35]. Therefore, understanding the electrostatic and steric forces generated by the selected NOM fractions would assist in predicting the interfacial interactions between NOM and capped AgNPs in electrolyte solutions, ultimately leading to colloidal stability or aggregation.

3.3. Aggregation kinetics of tannic acid-coated and silica-coated AgNPs in NOM-containing electrolyte solutions

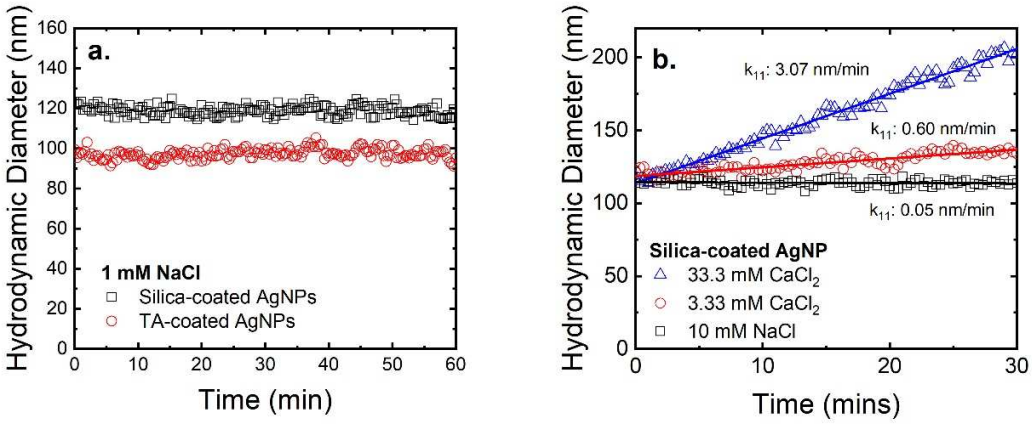

Figure 4: Aggregation kinetic of: a) Silica-coated and TA-coated AgNPs in 1 mM NaCl, and b) silica-coated AgNPs in 10 mM NaCl, 3.33 mM $CaCl_2$, and 33.3 mM $CaCl_2$.

The hydrodynamic diameter (D_h) of both silica-coated and TA-coated AgNPs was measured for 60 min in a 1 mM NaCl solution to determine their stability in solution and initial hydrodynamic diameters (D_{ho}) for further aggregation kinetics experiments (Figure 4a). Both types of nanoparticles showed high stability and a D_{ho} of 118.9±2.5 nm and 97.3±2.5 nm for silica-coated and TA-coated AgNPs, respectively. TA is a molecule (isoelectric point<2 and ~1.7 kDa)

commonly used for the stabilization of silver and gold nanoparticles in solution. In contrast, silica (isoelectric point~3) is a versatile coating option for nanomedicine, biodiagnostic, photothermal applications, and color. Also, silica preserves the optical properties and provides good salt stability to silver and gold nanoparticles. At environmentally relevant pH, both silica and TA acquire a negative charge, which would be fundamental during interactions with organics in solution.

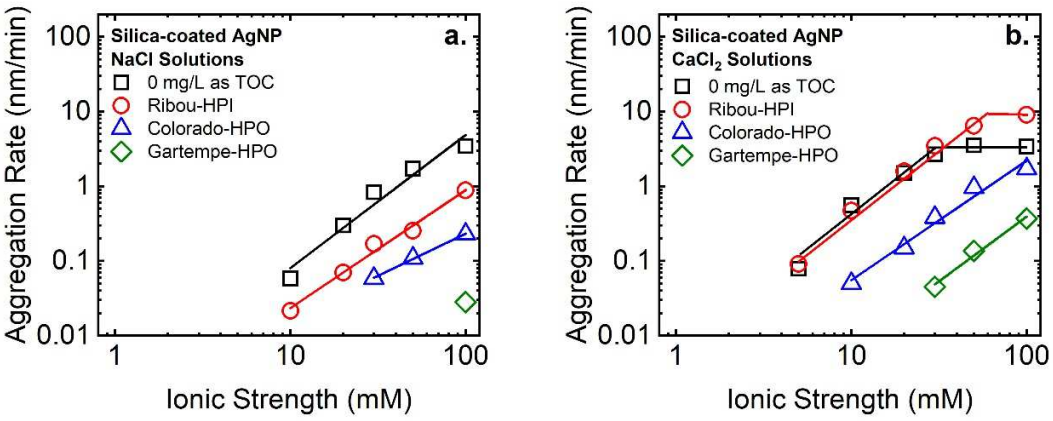

Figure 5: Aggregation kinetics of silica-coated AgNPs in a) NaCl and b) $CaCl_2$ solutions, in the absence and presence (10 mg C/L) of NOM

In the presence of increased NaCl concentration, the silica-coated AgNPs showed decreasing stability in solution due to simple charge screening (Figure S4). The aggregation rate (k_{11}) of silica-coated AgNPs increased from 0.05 to 0.30, 0.83, 1.72, and 3.43 nm/min for 10, 20, 30, 50 and 100 mM NaCl-containing solutions, respectively (Figure 4b and 5a, Table S3). No clear critical coagulation concentration (CCC) was observed at high ionic strength (IS). CCC is defined at the limit concentration between reaction-limited and diffusion-limited regimes [37]. On the other hand, the aggregation rates of silica-coated AgNPs in $CaCl_2$-containing solutions were slightly higher than those in NaCl, indicating the influence of cation bridging (i.e., specific interactions) on the destabilization of these nanoparticles (Figure 4b and 5b). The EPM of silica-

411 coated AgNPs in $CaCl_2$ was significantly lower than those in NaCl solution in the whole IS
412 tested; thus, confirming the latter observation. Specifically, at 1.66 mM $CaCl_2$ (5 mM IS) the k_{11}
413 was 0.08 nm/min and increased to 0.60, 1.50, 2.67, 3.52, and 3.07 nm/min at 3.33, 6.66, 10,
414 16.66, and 33.3 mM $CaCl_2$ (10, 20, 30, 50, and 100 mM IS), respectively (Table S3). Thus, CCC
415 was recorded at approximately 13.3 mM $CaCl_2$ (40 mM IS). Previous studies have observed bare
416 AgNPs to readily aggregate at low salt concentrations in solution (i.e., CCC<10 mM NaCl, and
417 CCC<1 mM $CaCl_2$); thus, mainly attributed to the low electrostatic stabilization of the bared Ag
418 surface [22, 50]. Therefore, the silica coating provided colloidal electrostatic stabilization to the
419 AgNPs.
420 Remarkably, in the presence of NOM-containing NaCl solution, the silica-coated AgNPs showed
421 enhanced stabilization. Nevertheless, the level of stabilization (k_{11}) highly depended on the
422 characteristics of the NOM. Briefly, the aggregation of silica-coated AgNPs in the presence of
423 Gartempe HPO was solely detected at 100 mM NaCl with a k_{11} of 0.03 nm/min, which was two
424 order of magnitude lower than the corresponding k_{11} (3.43 nm/min) in the absence of NOM
425 (Figure 5a). Colorado HPO also proved efficient in stabilizing silica-coated AgNPs at high ionic
426 strength; however, their aggregation rates were approximately 1.5 orders of magnitude lower
427 than those in the absence of NOM (Figure 5a). Additionally, no CCC was observed. On the other
428 hand, the presence of the hydrophilic fraction (Ribou HPI) also induced stability to the silica-
429 coated AgNPs, resulting in a 5-fold decrease of k_{11} compared to those in the absence of NOM
430 (Figure 5a). These results clearly indicate the adsorption of the organic fractions on the silica
431 capping (i.e., change in surface properties) and subsequent stabilization of the nanoparticles
432 through electrostatic and steric mechanisms. Interestingly, the level of stabilization of
433 nanoparticles in solution followed the same trend as observed during the AFM-EPM experiments

(Figures 2 and 3), where Gartempe HPO and Ribou HPI showed the highest and lowest repulsive forces, respectively. Specifically, Gartempe HPO adsorbed on silica-coated AgNPs would generate the highest energy barriers against successful collisions (i.e., and subsequent aggregation) through a combination of electrostatic and steric repulsive forces. These energy barriers would decrease with increasing NaCl concentration in solution due to simple charge screening (Na^+) and compression of polymeric structures. Conversely, among the three NOM selected, Ribou HPI showed the lowest and highest presence of carboxyl and alcoholic functional, respectively. Based on these characteristics, low electrostatic repulsive forces (i.e., inducing low energy barriers) and attractive acid-base interactions (occurring at short separation distances) would play a key role during the aggregation between silica-coated AgNPs in Ribou HPI-containing solutions. In brief, the most hydrophobic NOM fraction (Gartempe-HPO) provided the highest stability to silica-coated AgNPs in NaCl solutions based on electrosteric mechanisms. Remarkably, this stability decreased with increasing hydrophilicity of the NOM fraction due to lower electrostatic repulsion and attractive acid-base interactions occurring at short separation distances.

Remarkably, Ca^{2+} cations radically impacted the stability of silica-coated AgNPs in NOM-containing solutions (Figure 5b and S3b). The aggregation behavior was also highly dependent on the characteristics of the organic fractions. Briefly, aggregation of silica-coated AgNPs in Gartempe HPO-containing solutions was initially observed at 10 mM $CaCl_2$ (k_{11}: 0.05 nm/min) and increased with increasing $CaCl_2$ concentration (k_{11}: 0.37 nm/min at 33.3 mM $CaCl_2$); however, no CCC was observed. Similarly, the aggregation of silica-coated AgNPs in Colorado HPO-containing solutions was initially recorded at low divalent cation concentrations (3.3 mM $CaCl_2$) and showed a 7-fold increase in aggregation rates compared to those in NaCl.

Interestingly, at low $CaCl_2$ (i.e., 1.66, 3.33, and 10 mM $CaCl_2$), the aggregation rates of silica-coated AgNPs in Ribou HPI-containing solutions were similar to those in the absence of NOM. Nevertheless, at higher $CaCl_2$ concentrations (i.e., 16.6 and 33.3 mM $CaCl_2$), the presence of Ribou HPI induced enhanced aggregation in silica-coated AgNPs (Figure 5b). These results clearly indicated cation bridging as a dominant interaction mechanism between the deprotonated carboxyl groups in the organics adsorbed on the silica-coated AgNPs, and between organics and silica-coated AgNPs; thus, inducing aggregation. In a previous study, AFM was used to measure the adhesion forces between citrate-coated AgNPs and NOM in NaCl vs. $CaCl_2$-containing solutions, providing evidence of cation bridging mechanism [20]. Although it was not possible to confirm the full or partial NOM coating on the silica surface, the adsorption of these organic fractions changed the surface properties of the silica-coated AgNPs and was key for the stability and aggregation behavior of these nanoparticles in solution.

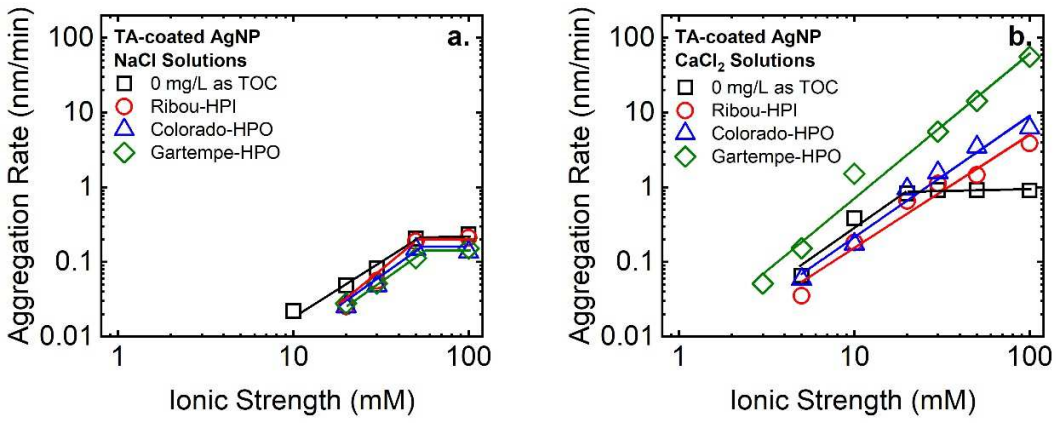

Figure 6: Aggregation kinetics of TA-coated AgNPs in a) NaCl and b) $CaCl_2$ solutions, in the absence and presence (10 mg C/L) of NOM

A low aggregation of TA-coated AgNPs (k_{11}: 0.02 nm/min) was observed in 10 mM NaCl. The aggregation rates increased with increasing NaCl in the solution until CCC was observed at approximately 50 mM NaCl (k_{11}: 0.20 nm/min) (Figure 6a and S3b). Remarkably the

475 aggregation rates of TA-coated AgNPs were approximately one order of magnitude lower than
476 those of silica-coated AgNPs under the same Na^+ concentration. The surface characteristics of
477 both types of nanoparticles played a crucial role in their aggregation behavior. Although the
478 EPM of both capped AgNPs were similar at low IS, the EPM of silica-coated AgNPs decreased
479 more with increasing IS than that of TA-coated AgNPs. This latter result indicates that ions exert
480 a higher impact on the surface of silica-coated AgNPs. Also, the silica coating is a hard and
481 smooth surface following classic DLVO interaction forces [35]. On the other hand, TA is an
482 organic molecule providing additional steric repulsive mechanisms due to its polymeric nature
483 [33, 47]. However, in $CaCl_2$ solutions of low concentrations (e.g., 3.33 to 10 mM $CaCl_2$), the
484 aggregation rates of TA-coated AgNPs were slightly one order of magnitude higher than those in
485 NaCl (Figure 6b and S3b). Also, a CCC was recorded at approximately 6.66 mM $CaCl_2$ (i.e., 20
486 mM ionic strength). These results indicate the impact of divalent cations through cation bridging
487 between deprotonated carboxyl groups in the TA structure; thus, inducing enhanced aggregation
488 and overcoming the steric mechanism provided by the polymeric structure of TA.[44]
489 Unlike silica-coated AgNPs, the presence of organics in solution did not radically change the
490 aggregation behavior of TA-coated AgNPs in NaCl-containing solutions (Figure 6a).
491 Specifically, the aggregation rates of TA-coated AgNPs slightly decreased in Gartempe HPO,
492 Colorado HPO, or Ribou HPI, and the CCC in these three conditions was still recorded at
493 approximately 50 mM NaCl. This latter observation indicates the low interactions between TA-
494 coated AgNPs and NOM in Na^+-containing solutions. Nevertheless, Ca^{2+} cations in solution
495 induced enhanced aggregation through cation bridging between deprotonated carboxyl groups on
496 the structure of both organic fractions and TA-coated AgNPs (Figure 6b and S3b). The changes
497 recorded in the aggregation rates were correlated to the characteristics of the organics in solution.

The magnitude of k_{11} across the tested $CaCl_2$ range followed the order of: Gartempe HPO > Colorado HPO > Ribou HPI. Based on their structures, the two HPO fractions (i.e., highly acidic in nature) present more carboxyl groups than the Ribou HPI fraction (i.e., where aliphatic structures and alcoholic groups are dominant in its structure). Additionally, the presence of carboxyl groups in the structure of organics has been commonly correlated to their EPM or zeta potential [20, 27]. Therefore, the high aggregation rates of TA-coated AgNPs in Gartempe HPO-containing solutions, exceeding those of Colorado HPO and Ribou HPI, would be caused by a higher content of deprotonated carboxyl group interacting through Ca^{2+} cations inner-sphere complexation with TA and Gartempe HPO molecules themselves [44]. Besides, no CCC was observed in the aggregation behavior of TA-coated AgNPs for the three organics tested, indicating reaction-limited aggregation even at higher $CaCl_2$ concentrations. These results clearly indicate the electrostatic and steric stabilization of AgNPs by the TA coating and the strong interactions between NOM and TA in Ca^{2+}-containing solutions, which ultimately impact the stability of the coated-nanoparticles.

4. Conclusions

The results presented in the current study introduce profound environmental implications. Silica and tannic acid are widely-used capping agents providing different surface properties to AgNPs as a function of their industrial target. Nevertheless, the release of these coated nanoparticles in the environment poses multiple threads to diverse aquatic ecosystems and human health. The experimental conditions in the current study tested the homoaggregation of capped nanoparticles under different solution chemistries and the presence of NOM. In natural aquifers, the aggregation of capped nanoparticles would be induced by colloids through heteroaggregation. Nevertheless, understanding the interactions between the capping agents and ubiquitous

components of the environment (e.g., NOM of different properties, cations, IS) is also crucial for understanding and predicting the fate and transport of capped-AgNPs in natural aquatic systems. The current results show that the physicochemical characteristics of the capping agents play a crucial role in the interfacial interactions with NOM and ions in solution. The hard and smooth surface of silica provided some stability in solution to the AgNPs (i.e., following classic DLVO mechanisms). However, this silica surface also showed strong interactions with both humic and non-humic organics in Na^+-containing solutions, ultimately deriving in NOM adsorption onto silica (i.e., change in surface properties), and enhanced stability. Humic NOMs provided more stability to the silica-coated AgNPs than its non-humic counterpart, mainly due to stronger electro-steric repulsive forces. Conversely, the polymeric TA provided higher stability to the AgNPs than silica coating and also showed weak interactions with NOM in the presence of Na^+ in solution. Ca^{2+} induced the aggregation of TA-coated and silica-coated AgNPs in NOM-containing solutions through specific interactions (i.e., cation bridging). However, humic NOM induced faster aggregation of both types of nanoparticles in Ca^{2+}-containing solutions due to its higher content of deprotonated carboxyl groups (i.e., cation bridging). These results indicate that: i) tannic acid as a capping agent, and ii) the adsorption of NOM onto the silica coating induce high stability in AgNPs. Due to the ubiquitous and dominant presence of humics in natural waters, the latter scenario would be highly possible. Remarkably, the aggregation rates of capped AgNPs would be correlated to the NOM concentration in the aquifers. In aquifers of high ionic strength and hardness (e.g., estuaries), the aggregation of these capped AgNPs would be expected, and their transport would be limited. Contrariwise, in freshwater (i.e., low ionic strength and presence of NOM), these capped nanoparticles would travel long distances. Nevertheless, different species would be preferentially affected by stable or aggregated AgNPs.

For instance, planktonic organisms in suspension would be more exposed to colloidally stable AgNPs, while benthic organisms living in sediments would be exposed to aggregated/sedimented AgNPs. The latter scenario is also fundamental during the risk assessment of AgNPs in natural aquatic systems.

Acknowledgments

The authors are grateful to Dr. Denise Mitrano for providing the Ag nanoparticle samples.

References

[1] N. Singh, B. Manshian, G.J.S. Jenkins, S.M. Griffiths, P.M. Williams, T.G.G. Maffeis, C.J. Wright, S.H. Doak, NanoGenotoxicology: The DNA damaging potential of engineered nanomaterials, Biomaterials, 30 (2009) 3891-3914.
[2] M. Ahamed, M.S. AlSalhi, M.K.J. Siddiqui, Silver nanoparticle applications and human health, Clin. Chim. Acta, 411 (2010) 1841-1848.
[3] S.A. Blaser, M. Scheringer, M. MacLeod, K. Hungerbühler, Estimation of cumulative aquatic exposure and risk due to silver: Contribution of nano-functionalized plastics and textiles, Sci. Total Environ., 390 (2008) 396-409.
[4] J. Gao, K. Powers, Y. Wang, H. Zhou, S.M. Roberts, B.M. Moudgil, B. Koopman, D.S. Barber, Influence of Suwannee River humic acid on particle properties and toxicity of silver nanoparticles, Chemosphere, 89 (2012) 96-101.
[5] C. Gil-Allué, K. Schirmer, A. Tlili, M.O. Gessner, R. Behra, Silver Nanoparticle Effects on Stream Periphyton During Short-Term Exposures, Environ. Sci. Technol., 49 (2015) 1165-1172.
[6] B.P. Colman, B. Espinasse, C.J. Richardson, C.W. Matson, G.V. Lowry, D.E. Hunt, M.R. Wiesner, E.S. Bernhardt, Emerging Contaminant or an Old Toxin in Disguise? Silver Nanoparticle Impacts on Ecosystems, Environ. Sci. Technol., 48 (2014) 5229-5236.
[7] C. Levard, E.M. Hotze, B.P. Colman, A.L. Dale, L. Truong, X.Y. Yang, A.J. Bone, G.E. Brown, R.L. Tanguay, R.T. Di Giulio, E.S. Bernhardt, J.N. Meyer, M.R. Wiesner, G.V. Lowry, Sulfidation of Silver Nanoparticles: Natural Antidote to Their Toxicity, Environ. Sci. Technol., 47 (2013) 13440-13448.
[8] K.L. Chen, M. Elimelech, Aggregation and deposition kinetics of fullerene (C-60) nanoparticles, Langmuir, 22 (2006) 10994-11001.
[9] T. Cosgrove, Colloid Science: Principles, Methods and Applications, Wiley, 2010.
[10] T. Phenrat, N. Saleh, K. Sirk, H.-J. Kim, R.D. Tilton, G.V. Lowry, Stabilization of aqueous nanoscale zerovalent iron dispersions by anionic polyelectrolytes: adsorbed anionic polyelectrolyte layer properties and their effect on aggregation and sedimentation, J Nanopart Res, 10 (2008) 795-814.
[11] E.M. Hotze, T. Phenrat, G.V. Lowry, Nanoparticle aggregation: challenges to understanding transport and reactivity in the environment, J. Environ. Qual., 39 (2010) 1909-1924.
[12] A.M.E. Badawy, T.P. Luxton, R.G. Silva, K.G. Scheckel, M.T. Suidan, T.M. Tolaymat, Impact of Environmental Conditions (pH, Ionic Strength, and Electrolyte Type) on the Surface Charge and Aggregation of Silver Nanoparticles Suspensions, Environ. Sci. Technol., 44 (2010) 1260-1266.
[13] B.J.R. Thio, M.O. Montes, M.A. Mahmoud, D.-W. Lee, D. Zhou, A.A. Keller, Mobility of Capped Silver Nanoparticles under Environmentally Relevant Conditions, Environ. Sci. Technol., 46 (2011) 6985-6991.

583 [14] M. Tejamaya, I. Römer, R.C. Merrifield, J.R. Lead, Stability of Citrate, PVP, and PEG Coated Silver
584 Nanoparticles in Ecotoxicology Media, Environ. Sci. Technol., 46 (2012) 7011-7017.
585 [15] Y. Cao, R. Zheng, X. Ji, H. Liu, R. Xie, W. Yang, Syntheses and characterization of nearly
586 monodispersed, size-tunable silver nanoparticles over a wide size range of 7–200 nm by tannic acid
587 reduction, Langmuir, 30 (2014) 3876-3882.
588 [16] H. Choi, J.-P. Lee, S.-J. Ko, J.-W. Jung, H. Park, S. Yoo, O. Park, J.-R. Jeong, S. Park, J.Y. Kim,
589 Multipositional Silica-Coated Silver Nanoparticles for High-Performance Polymer Solar Cells, Nano
590 Letters, 13 (2013) 2204-2208.
591 [17] S. Liu, Z. Zhang, M. Han, Gram-Scale Synthesis and Biofunctionalization of Silica-Coated Silver
592 Nanoparticles for Fast Colorimetric DNA Detection, Analytical Chemistry, 77 (2005) 2595-2600.
593 [18] S.K. Sivaraman, I. Elango, S. Kumar, V. Santhanam, A green protocol for room temperature synthesis
594 of silver nanoparticles in seconds, Current Science (00113891), 97 (2009).
595 [19] S.A. Cumberland, J.R. Lead, Particle size distributions of silver nanoparticles at environmentally
596 relevant conditions, J. Chromatogr. A, 1216 (2009) 9099-9105.
597 [20] L. Gutierrez, C. Aubry, M. Cornejo, J.-P. Croue, Citrate-Coated Silver Nanoparticles Interactions with
598 Effluent Organic Matter: Influence of Capping Agent and Solution Conditions, Langmuir, 31 (2015) 8865-
599 8872.
600 [21] M. Delay, T. Dolt, A. Woellhaf, R. Sembritzki, F.H. Frimmel, Interactions and stability of silver
601 nanoparticles in the aqueous phase: Influence of natural organic matter (NOM) and ionic strength, J.
602 Chromatogr. A, 1218 (2011) 4206-4212.
603 [22] X. Li, J.J. Lenhart, H.W. Walker, Dissolution-Accompanied Aggregation Kinetics of Silver
604 Nanoparticles, Langmuir, 26 (2010) 16690-16698.
605 [23] S.L. Chinnapongse, R.I. MacCuspie, V.A. Hackley, Persistence of singly dispersed silver nanoparticles
606 in natural freshwaters, synthetic seawater, and simulated estuarine waters, Sci. Total Environ., 409
607 (2011) 2443-2450.
608 [24] K.A. Huynh, K.L. Chen, Aggregation Kinetics of Citrate and Polyvinylpyrrolidone Coated Silver
609 Nanoparticles in Monovalent and Divalent Electrolyte Solutions, Environ. Sci. Technol., 45 (2011) 5564-
610 5571.
611 [25] H.M. Chen, C.F. Hsin, R.-S. Liu, J.-F. Lee, L.-Y. Jang, Synthesis and Characterization of Multi-Pod-
612 Shaped Gold/Silver Nanostructures, The Journal of Physical Chemistry C, 111 (2007) 5909-5914.
613 [26] Z. Yi, X. Li, X. Xu, B. Luo, J. Luo, W. Wu, Y. Yi, Y. Tang, Green, effective chemical route for the
614 synthesis of silver nanoplates in tannic acid aqueous solution, Colloids Surf., A, 392 (2011) 131-136.
615 [27] C. Aubry, L. Gutierrez, J.P. Croue, Coating of AFM probes with aquatic humic and non-humic NOM
616 to study their adhesion properties, Water Res., 47 (2013) 3109-3119.
617 [28] L. Gutierrez, C. Aubry, R. Valladares Linares, J.-P. Croue, Natural organic matter interactions with
618 polyamide and polysulfone membranes: Formation of conditioning film, Colloids Surf., A, 477 (2015) 1-8.
619 [29] J.A. Leenheer, J.-P. Croué, M. Benjamin, V. Korshin Gregory, J. Hwang Cordelia, A. Bruchet, R. Aiken
620 George, Comprehensive Isolation of Natural Organic Matter from Water for Spectral Characterizations
621 and Reactivity Testing, in: Natural Organic Matter and Disinfection By-Products, American Chemical
622 Society, 2000, pp. 68-83.
623 [30] C. Hwang, S.W. Kranser, G. Amy, A. Bruchet, J.P. Croue, A. Leenheer Jerry, Polar NOM:
624 Characterization, DBPs, Treatment, AWWA Research Foundation, 2001.
625 [31] J.A. Leenheer, J.P. Croué, Characterizing aquatic dissolved organic matter, Environ. Sci. Technol., 37
626 (2003) 18A-26A.
627 [32] L. Gutierrez, T.H. Nguyen, Interactions between rotavirus and natural organic matter isolates with
628 different physicochemical characteristics, Langmuir, 29 (2013) 14460-14468.

[33] S. Sander, L.M. Mosley, K.A. Hunter, Investigation of Interparticle Forces in Natural Waters: Effects of Adsorbed Humic Acids on Iron Oxide and Alumina Surface Properties, Environ. Sci. Technol., 38 (2004) 4791-4796.
[34] H.J. Butt, B. Cappella, M. Kappl, Force measurements with the atomic force microscope: Technique, interpretation and applications, Surf. Sci. Rep., 59 (2005) 1-152.
[35] J.N. Israelachvili, Intermolecular and Surface Forces: Revised Third Edition, Elsevier Science, 2011.
[36] L.S. Dorobantu, S. Bhattacharjee, J.M. Foght, M.R. Gray, Analysis of Force Interactions between AFM Tips and Hydrophobic Bacteria Using DLVO Theory, Langmuir, 25 (2009) 6968-6976.
[37] S.E. Mylon, C.I. Rinciog, N. Schmidt, L. Gutierrez, G.C.L. Wong, T.H. Nguyen, Influence of Salts and Natural Organic Matter on the Stability of Bacteriophage MS2, Langmuir, 26 (2010) 1035-1042.
[38] G. Makdissy, J.-P. Croué, G. Amy, H. Buisson, Fouling of a polyethersulfone ultrafiltration membrane by natural organic matter, Water Science and Technology: Water Supply, 4 (2004) 205-212.
[39] F.L. Rosario-Ortiz, S.A. Snyder, I.H. Suffet, Characterization of dissolved organic matter in drinking water sources impacted by multiple tributaries, Water Res., 41 (2007) 4115-4128.
[40] A.G. Kalinichev, R.J. Kirkpatrick, Molecular dynamics simulation of cationic complexation with natural organic matter, Eur. J. Soil Sci., 58 (2007) 909-917.
[41] J.A. Brant, K.M. Johnson, A.E. Childress, Characterizing NF and RO membrane surface heterogeneity using chemical force microscopy, Colloids Surf., A, 280 (2006) 45-57.
[42] A.E. Contreras, Z. Steiner, J. Miao, R. Kasher, Q. Li, Studying the Role of Common Membrane Surface Functionalities on Adsorption and Cleaning of Organic Foulants Using QCM-D, Environ. Sci. Technol., 45 (2011) 6309-6315.
[43] L. Gutierrez, T.H. Nguyen, Interactions between Rotavirus and Suwannee River Organic Matter: Aggregation, Deposition, and Adhesion Force Measurement, Environ. Sci. Technol., 46 (2012) 8705-8713.
[44] A.G. Kalinichev, E. Iskrenova-Tchoukova, W.-Y. Ahn, M.M. Clark, R.J. Kirkpatrick, Effects of Ca2+ on supramolecular aggregation of natural organic matter in aqueous solutions: A comparison of molecular modeling approaches, Geoderma, 169 (2011) 27-32.
[45] L. Gutierrez, C. Aubry, L. Dramas, P. Aimar, J.-P. Croue, Characterization of Skeletonema costatum intracellular organic matter and study of nanomechanical properties under different solution conditions, Colloids Surf., A, 506 (2016) 154-161.
[46] X. Li, B.E. Logan, Analysis of bacterial adhesion using a gradient force analysis method and colloid probe atomic force microscopy, Langmuir, 20 (2004) 8817-8822.
[47] L.M. Mosley, K.A. Hunter, W.A. Ducker, Forces between Colloid Particles in Natural Waters, Environ. Sci. Technol., 37 (2003) 3303-3308.
[48] H. Yamamura, K. Kimura, T. Okajima, H. Tokumoto, Y. Watanabe, Affinity of functional groups for membrane surfaces: Implications for physically irreversible fouling, Environ. Sci. Technol., 42 (2008) 5310-5315.
[49] T.L. Byrd, J.Y. Walz, Interaction force profiles between Cryptosporidium parvum oocysts and silica surfaces, Environ. Sci. Technol., 39 (2005) 9574-9582.
[50] A.M. El Badawy, K.G. Scheckel, M. Suidan, T. Tolaymat, The impact of stabilization mechanism on the aggregation kinetics of silver nanoparticles, Sci. Total Environ., 429 (2012) 325-331.